

Article

# Novel Preparation of Noncovalent Modified GO Using RAFT Polymerization to Reinforce the Performance of Waterborne Epoxy Coatings

Baolei Liu <sup>1</sup>, Mingqian Wang <sup>1</sup>, Ying Liang <sup>1</sup>, Zhicheng Zhang <sup>1</sup>, Guohong Ren <sup>1</sup>, Yajun Liu <sup>1</sup>, Shishan Wu <sup>1,\*</sup>  and Jian Shen <sup>1,2</sup>

<sup>1</sup> School of Chemistry and Chemical Engineering, Nanjing University, 163 Xianlin Avenue, Qixia District, Nanjing 210023, China; dg1824046@smail.nju.edu.cn (B.L.); dg1624064@smail.nju.edu.cn (M.W.); mg1724050@smail.nju.edu.cn (Y.L.); mg1724101@smail.nju.edu.cn (Z.Z.); dg1624054@smail.nju.edu.cn (G.R.); mf1624019@smail.nju.edu.cn (Y.L.); shenj57@nju.edu.cn (J.S.)

<sup>2</sup> Jiangsu Collaborative Innovation Center of Biomedical Functional Materials, Jiangsu Key Laboratory of Biomedical Materials, College of Chemistry and Materials Science, Nanjing Normal University, Nanjing 210046, China

\* Correspondence: shishanwu@nju.edu.cn; Tel.: +86-25-8331-6661

Received: 4 May 2019; Accepted: 25 May 2019; Published: 28 May 2019



**Abstract:** This work launches the first-ever report on the fabrication of waterborne epoxy-graphene oxide (GO) coatings (WEGC) using a block polymer as a dispersant of GO, wherein the block polymer was synthesized via reversible addition-fragmentation chain transfer (RAFT) polymerization of acrylic acid and oligo(ethylene glycol) methyl ether methacrylate. A number of analytical techniques, such as Fourier transform infrared spectroscopy (FTIR), scanning electron microscopy (SEM), X-ray diffraction (XRD), thermo gravimetric analysis (TGA), and salt spray tests, were utilized to explore the morphology and performance of the WEGC. It was confirmed that POEGMA950-*b*-PAA attached to the GO nanosheets, increasing the integral space of the sheets. Modified GO (MGO) layers were well-dispersed in the epoxy matrix through the formation of a GO-dispersant-epoxy ternary molecular structure. Furthermore, the presence of MGO substantially influenced the thermal properties, mechanical properties, and anticorrosion performance of the WEGC. TGA, salt spray tests, and pull-off tests showed that 0.5 wt.% MGO content achieved the greatest improvement in the evaluated properties.

**Keywords:** graphene oxide; RAFT polymerization; waterborne epoxy coating; anticorrosion

## 1. Introduction

Organic coatings are widely used in corrosion protection, as they can provide an efficient physical barrier between metal surfaces and a corrosive environment [1,2]. However, at present, most anticorrosion coatings are typical solvent-borne systems. The high percentage of volatile compounds (VOCs) they contain is extremely harmful to the environment and human health [3]. Therefore, waterborne coatings have gained significant attention world-wide with the consideration of environmental protection [4–6].

Recently, a variety of types of water-soluble and dispersible polymeric resins, such as acrylics, polyesters, epoxies, polyurethanes, and alkyd resins, have been developed for waterborne coating formulations [7–9]. Waterborne epoxy coatings are the most studied primers due to their strong adhesion to metallic substrates, low curing shrinkage and high chemical stability [10–13]. However, cured waterborne epoxy coatings contain a lot of polar channels, which result from residual surfactants or hydrophilic groups. These channels accelerate water permeation and water uptake. More seriously,

this can lead to deterioration of the coating matrix, there by initiating corrosion. Consequently, there are many defects in waterborne epoxy coatings, such as flash-rust, poor adhesion, and poor water resistance [14–16], and the anticorrosion performance of waterborne epoxy coatings is much poorer than solvent-borne epoxy coatings. The introduction of nanofillers or nanopigment can decrease coating defects by filling in pores and cavities. A number of nanofillers, such as ZnO, Al<sub>2</sub>O<sub>3</sub>, SiO<sub>2</sub>, and TiO<sub>2</sub>, have been successfully utilized to improve the performance of waterborne coatings [10].

Graphene, which has two-dimensional structures of thickness equal to a single-atom, has gained enormous attention since its discovery by Novoselov et al. [17]. It has great potential to improve the performance of anticorrosion coatings, as it can provide chemical inertness and barrier properties against the penetration of oxygen, water, and corrosive ions [18–21]. However, high specific surface area, strong  $\pi$ - $\pi$  interactions, and strong van der Waals forces between graphene layers results in their stacking form, limiting graphene's further processing in applications [10]. Therefore, delamination and distribution of graphene in a coating matrix plays an important role in the preparation of graphene composites [22,23]. Graphene oxide (GO), with the presence of carboxylic, hydroxyl, and epoxy functional groups, is a vital derivative of graphene. Since its nanosheets functionalize (covalent or noncovalent) more easily and the corresponding functionalization product has better compatibility with polymers, GO could be an attractive alternative for graphene. Zhu et al. synthesized a water-dispersible graphene (PG) by a nucleophilic ring-opening reaction of the primary amine group in 3-(1-(2-aminopropoxy) propan-2-ylamino) propane-1-sulfonate sodium with epoxy groups on the basal plane of GO, followed by in situ reduction with hydrazine hydrate. Then, the product was employed as an anoscale reinforcement filler in waterborne acrylic-modified alkyd resin coatings. The authors reported that the stability and corrosion resistance of the composite materials reached an optimum when the content of PG was set to 1% [24]. Yet et al. prepared polyaniline (PANI)/GO coatings with superior performance, which used PANI to covalently modify GO [19].

Graphene oxide's covalent functionalization invariably produces defect sites in its conjugated sheet-structured graphene and compromises its dispersion [25]. Consequently, a lot of researches have attempted to enhance GO dispersion by noncovalent polymer functionalization. Polymeric dispersant is one of the most effective noncovalent approaches to achieve stable aqueous suspensions of GO [26–30]. Hayatgheib et al. prepared GO-PANI/epoxy coatings by applying PANI to functionalize GO. The introduction of PANI nanofibers deposited on the GO sheets greatly improved the compatibility of GO with the epoxy resin. Furthermore, it enhanced the thermal stability, protection, and barrier properties of the coating [31]. Ramezanzadeh et al. successfully functionalized GO using an aromatic diamine. They reported that the functionalized GO dispersed excellently in the epoxy matrix, and that the corrosion resistance properties of the corresponding products were reinforced [32]. There is a critical challenge to design and prepare efficient polymeric dispersants with facile synthesis routes to disperse GO in a waterborne epoxy matrix and achieve long-term anticorrosion.

Reversible addition-fragmentation chain transfer (RAFT) polymerization is a versatile and powerful method of preparing complex molecular architectures, for instance, block, graft, gradient, comb, and star copolymers. Not only is it compatible with a wide range of monomers, it is also environmentally friendly and requires mild polymerization conditions. Thus, RAFT polymerization—with the introduction of a suitable RAFT agent—is similar to a conventional free radical polymerization reaction [33]. In our previous work, the block polymer, which contained both poly[oligo(ethylene glycol) ether acrylate] (POEGA) and poly(acrylic acid) (PAA) structures, was prepared by RAFT polymerization in an aqueous medium. It was confirmed that it could significantly improve the dispersion of GO and multi-wall carbon nanotubes (MWCNTs) [33,34].

As far as we know, this work launches the first ever report on the fabrication of waterborne epoxy-GO coatings (WEGC) using a block polymer as a dispersant of GO, wherein the block polymer was synthesized via RAFT polymerization of acrylic acid and oligo (ethylene glycol) methyl ether methacrylate (OEGMA). Various analytical methods, such as Fourier transform infrared spectroscopy (FTIR), scanning electron microscopy (SEM), X-ray diffraction (XRD), thermogravimetric analysis (TGA),

water absorption rate determination, and salt spray tests, were employed to explore the morphology of GO in an epoxy matrix and the anticorrosion mechanism of the WEGC. It is demonstrated that GO was uniformly dispersed in the epoxy matrix with the help of POEGMA950-*b*-PAA, and that the well-dispersed modified graphene oxide (MGO) substantially improved both the mechanical properties and anticorrosion performance of the organic paints considered.

## 2. Materials and Methods

### 2.1. Materials

Experimental 4,4'-azobis(4-cyanovaleric acid) (ACVA), oligo(ethylene glycol) methyl ether methacrylate (OEGMA950;  $M_n = 950$  g/mol), and 4-cyano-4-(phenylcarbonothioylthio) pentanoic acid (CPA) were purchased from Sigma-Aldrich (Saint Louis, MO, USA). Acrylic acid, sodium acetate, acetic acid,  $\text{NaHCO}_3$ ,  $\text{NaNO}_3$ ,  $\text{H}_2\text{SO}_4$ ,  $\text{KMnO}_4$ ,  $\text{H}_2\text{O}_2$ , and HCl were purchased from Nanjing Chemical Reagent Co. Graphite (Nanjing, China, flakes, 99% carbon basis, 325 mesh particle size  $\geq 99\%$ , natural) was purchased from Sigma-Aldrich. The two-component waterborne epoxy coating was purchased from Jiangsu Changjiang Paint Co., Ltd (Nanjing, China). The non-volatile-matter contents of the paint and the curing agent were 55.3% and 40% in weight, respectively. The epoxy resin content of the paint was 20.5%. The mixing ratio of paint to curing agent was 10:1 in weight. All reagents were used as received.

### 2.2. Synthesis of Poly[oligo(Ethylene Glycol) Methyl Ether Methacrylate] (POEGMA950-RAFT)

POEGMA950-*b*-PAA was prepared via RAFT polymerization following similar procedures to those described in our previous work [33]. Precisely 6.0 g of OEGMA950 was added to 34.0 mL acetate buffer (1 mol/L, pH = 5.2) containing 0.004 g ACVA and 0.04 g CPA. Prior to polymerization, the solution was purged with nitrogen for 30 min. Then, it was heated to 70 °C in a thermostatically controlled oil bath under stirring. The flask was immersed in iced water after 10 h to quench the polymerization. The product was then dialyzed against water and dried in vacuum ( $M_n = 1.94 \times 10^4$  g/mol, PDI = 1.23).

### 2.3. Synthesis of POEGMA950-Block-PAA (POEGMA950-*b*-PAA)

The polymerization of acrylic acid was carried out in  $\text{NaHCO}_3$  aqueous solution (0.01 mol/L) with 2.0 g POEGMA950-RAFT, 0.0023 g ACVA, and 0.36 g acrylic acid. Prior to polymerization, the solution was purged with nitrogen for 30 min. Then, it was heated to 70 °C in a thermostatically controlled oil bath under stirring for 5 h. The product was then dialyzed and dried in vacuum ( $M_n = 2.34 \times 10^4$  g/mol, PDI = 1.35).

### 2.4. Preparation of GO by Oxidation of Graphite

GO was prepared by graphite oxidation using a modified Hummers' method [35].  $\text{NaNO}_3$  (3.0 g) and graphite (6.0 g) were mixed with  $\text{H}_2\text{SO}_4$  (360 mL) under stirring for 15 min.  $\text{KMnO}_4$  (18.0 g) was added slowly to the flask under stirring at 35 °C for 7 h. Then, the second part of  $\text{KMnO}_4$  (18.0 g) was added and stirring was continued for 12 h.  $\text{H}_2\text{O}_2$  (30 vol.%, 60 mL) and deionized water (1200 mL) were added to reduce the remaining  $\text{KMnO}_4$ . The obtained solution was centrifuged. The paste was washed with HCl solution (10 vol.%) and distilled water. The obtained product was dispersed in 100 mL distilled water. Then, the graphite oxide dispersion was exfoliated by probe ultrasonic for 30 min with a frequency of 50 Hz, filtered and dried (by freeze drying) to get the GO powder.

### 2.5. Preparation of Modified GO (MGO)

GO (50 mg) was dispersed in 50 mL aqueous solution of POEGMA950-*b*-PAA (1 mg/mL) with the assistance of sonication for 30 min. A non-attached block polymer was removed by filtering. Then, the dispersion was dried by freeze drying. The obtained block polymer and GO composite was designated as MGO.

## 2.6. Preparation of the Waterborne Epoxy-GO Coatings (WEGC)

The obtained MGO was added to two-component waterborne epoxy coatings (0.1, 0.5, and 1.0 wt.% with respect to epoxy resin). The mixtures were first stirred for 30 min and then degassed in a vacuum oven at 25 °C. The coatings were designated as WEGC-G1 (0.1 wt.% GO), WEGC-G5 (0.5 wt.% GO), and WEGC-G10 (1.0 wt.% GO) based on their weight content of MGO. For comparison, WEGC-G0 (without any GO addition) was prepared in similar procedures.

The substrates (Q235 steel) were abraded by 500 grit sand paper, degreased ultrasonically in acetone, and dried at 50 °C. The WEGC were coated on the processed substrates by air spray with a nozzle pressure of 0.5 MPa, and were dried at 120 °C for 2 h. They were then dried at 25 °C for 7 days, prior to the test. The thickness of the dry-films was  $51 \pm 2 \mu\text{m}$ , measured by QNIX 4500 coating thickness gauges. The preparation process of the WEGC is exhibited in Figure 1.

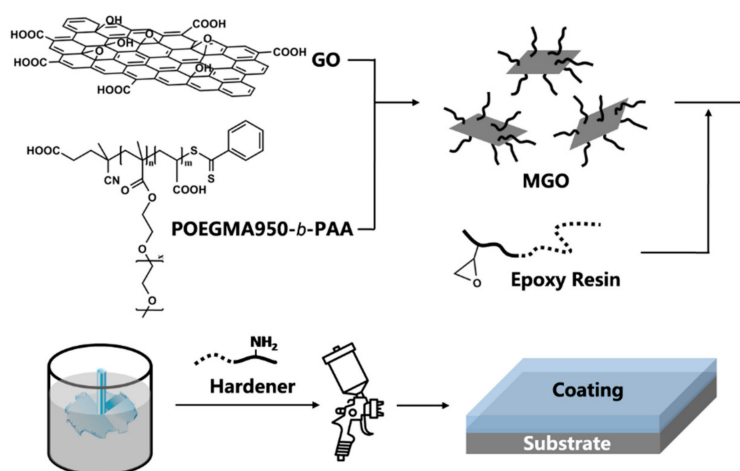


**Figure 1.** Schematic illustration of the preparation of the waterborne epoxy-graphene oxide coatings (WEGC).

## 2.7. Characterization

Fourier transform infrared spectroscopy (FTIR) was carried out on a Bruker spectrometer (Billerica, MA, USA) at a resolution of  $4 \text{ cm}^{-1}$ . An average of 24 scans were taken per sample using the KBr pellet technique. Gel permeation chromatography (GPC, Agilent 1260 HPLC) was carried out with 0.1 mol/L  $\text{NaNO}_3$  aqueous solution as the eluent at a flow rate of 1 mL/min. Raman spectra were measured with a confocal Raman spectrometer (Renishawinvia Reflex, Wotton-under-Edge, UK) using a wavelength of 533 nm. Scanning electron microscopy (SEM, FEI Quanta 250, Hillsboro, OR, USA) was conducted to characterize the surface morphology of the GO, and the fracture surface of the coatings. X-ray diffraction (XRD) was performed on step-scan mode by an X-ray diffractometer (Bruker D8-advance) equipped with  $\text{Cu K}\alpha$  radiation ( $\lambda = 0.1540 \text{ nm}$ ). In the test of GO and MGO, the scanning rate was  $4^\circ$  per minute. In the test of the WEGC, the scanning rate was  $0.5^\circ$  per minute. The thermal property of the epoxy coatings was evaluated by TGA (TGA-7 analyzer, PerkinElmer, Waltham, MA, USA) with a heating rate of  $10^\circ\text{C}/\text{min}$  from 25 to  $600^\circ\text{C}$  under nitrogen.

## 2.8. Salt Spray Tests

The anticorrosion property of the WEGC was investigated using a salt spray test in accordance with ASTM B117 [36] and ASTM D714 [37]. Prior to the test, scribes were created on the surface of the WEGC using a surgery knife. Samples were placed in a salt spray cabinet at  $35^\circ\text{C}$  with continuous spray of NaCl solution (5.0 wt.%, pH = 6.5–7.0). Three parallel tests were carried out for all samples.

### 2.9. Determination of the Water Absorption Rate

The WEGC were coated on aluminum substrates using an air spray with a nozzle pressure of 0.5 MPa. They were dried for 2 h at 120 °C, and then a further 7 days at 25 °C. The thickness of the dry-films was  $30 \pm 2 \mu\text{m}$ , measured by QNIX 4500 coating thickness gauges. These samples were then immersed vertically in distilled water. After reaching the prescribed time, these samples were taken out and their surfaces dried using filter paper. The samples were then weighed to calculate the water absorption rate. Three parallel tests were carried out for all samples.

### 2.10. Pull-Off Test

The adhesion of the WEGC on Q235 steel was determined using a pull-off adhesion tester (Biuged BGD 500, Guangzhou, China) according to ASTM D4541 [38]. Prior to the test, the substrates and steel dollies were abraded by 120# sand paper to achieve a roughness of 25–50  $\mu\text{m}$ . Three parallel tests were carried out for all samples.

## 3. Results and Discussion

The FTIR spectra of GO, POEGMA950-*b*-PAA, and MGO are shown in Figure 2a. The peaks observed in the GO spectrum at 1223, 1710, 1062 and 859  $\text{cm}^{-1}$ , and 1633  $\text{cm}^{-1}$  are assigned to C–OH stretching vibration, C=O stretching vibration, C–O vibration of epoxy groups, and C=C vibration of aromatic rings, respectively [39]. In the FTIR spectrum of POEGMA950-*b*-PAA, the observed peaks are assigned to C–O–C stretching (857  $\text{cm}^{-1}$ ), C–H bending in –O–CH<sub>3</sub> (943  $\text{cm}^{-1}$ ), C–O stretching (1118  $\text{cm}^{-1}$ ), –CH<sub>2</sub>– bending (1459 and 1340  $\text{cm}^{-1}$ ), C=O stretching (1737  $\text{cm}^{-1}$ ), C–H stretching (2870  $\text{cm}^{-1}$ ), and O–H vibration (3000  $\text{cm}^{-1}$ ). The FTIR spectrum of MGO clearly shows the characteristic C–H stretching (2870  $\text{cm}^{-1}$ ) and –CH<sub>2</sub>– bending (1340  $\text{cm}^{-1}$ ) (Figure 2a, marked by arrows), suggesting that the POEGMA950-*b*-PAA chains noncovalently connected to the surface of GO.

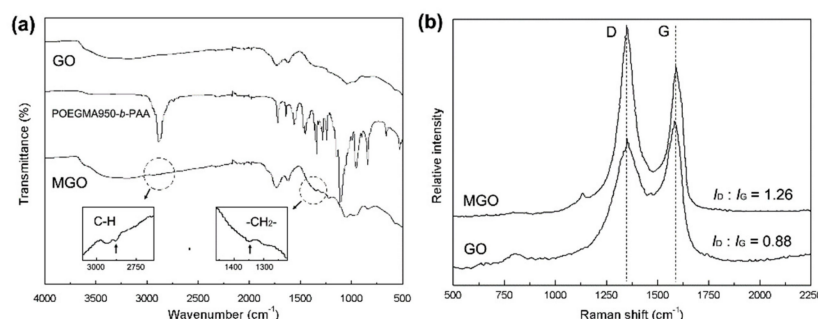


**Figure 2.** (a) Fourier transform infrared spectroscopy (FTIR) spectra and (b) Raman spectra of products.

The Raman spectra provided additional evidence of the noncovalent connection between the block copolymer and the GO surface. As presented in Figure 2b, two prominent bands can be observed at 1580 and 1335  $\text{cm}^{-1}$ . The band at 1335  $\text{cm}^{-1}$  (D band) arises due to the vibration of carbon atoms in disordered graphite, indicating the formation of  $sp^3$  carbon in the GO. The band at 1580  $\text{cm}^{-1}$  (G band) is associated with the first order scattering of the  $E_{2g}$  vibration mode for a  $sp^2$  carbon lattice in the graphitic domain [40]. Generally, the defect density or the disorder extent of GO composites can be characterized by the intensity ratio of the D and G bands ( $I_D/I_G$ ) [41]. In our tests, the  $I_D/I_G$  ratio of GO was 0.88. After polymeric functionalization of POEGMA950-*b*-PAA, the  $I_D/I_G$  ratio gradually increased to 1.26. Additionally, the  $sp^3$  carbon structure of GO increased with the presence of POEGMA950-*b*-PAA, which resulted from a noncovalent linkage between GO and the POEGMA950-*b*-PAA chains [42].

X-ray diffraction (XRD) was used to determine the composition and crystal structure of the GO, MGO, and WEGC. The diffraction peaks ( $2\theta$ ) of GO and MGO appeared at 10.85° and 8.77°, respectively (Figure 3a). The values corresponded to a basal spacing ( $d_{001}$ ) of 0.835 and 1.01 nm. The reflection of the MGO (001) planes weakened and shifted to lower angles after modification with

POEGMA950-*b*-PAA. The presence of POEGMA950-*b*-PAA increased the integral space of the GO sheets by attaching to their surface, resulting in a proper degree of intercalation of the GO nanosheets. Noncovalently grafted POEGMA950-*b*-PAA chains on the GO surface markedly increased the full width of the peak (at the half maximum position) due to the increase in *d*-spacing between the GO sheets [43]. This indicated that the disordered structure of the nanolayers resulted from sonication and noncovalent functionalization processes.

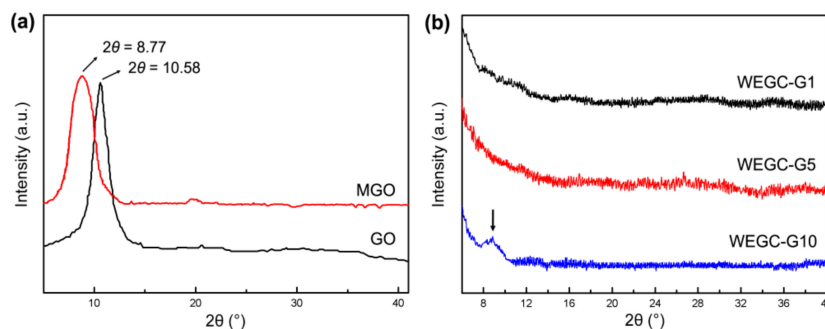


**Figure 3.** X-ray diffraction (XRD) patterns of (a) graphene oxide (GO), modified graphene oxide (MGO), and (b) waterborne epoxy-GO coatings (WEGC).

No additional diffraction peaks were found in the XRD patterns of WEGC-G1 or WEGC-G5 (Figure 3b). In Figure 3b, it is demonstrated that WEGC-G1 and WEGC-G5 do not present ordering anymore or the spacing between the MGO layers is too large (i.e., exceeding 8 nm in the case of ordered exfoliated structure) [44]. In contrast, there is a broad peak (Figure 3b, black arrow) in the XRD patterns of WEGC-G10. This means that some of the exfoliated MGO layer rearranged in the coating with higher MGO content.

The morphology of MGO obtained by noncovalent functionalization was directly observed by SEM (Figure 4c,d). The SEM images of MGO showed that the GO layer was very thin and contained some wrinkles. This phenomenon was possibly due to the strong interactions between sonication and the organic polymer chains. These wrinkles may have had an important role in preventing aggregation of GO and maintaining high surface area [45]. Furthermore, the influence of GO nanosheets on the morphological properties of the epoxy coating was investigated. Figure 4e shows the fracture surface of the waterborne epoxy coating (WEGC-G0). These surfaces are almost smooth, possessing only sharp cracks, indicating the mechanical properties of the WEGC-G0 coating are poor. The coating's stress damping behavior is weak and the applied stress concentrates at some weak and defect parts of the coating, resulting in the growth of cracks [46]. In contrast, the fracture surfaces of the WEGC with added GO (Figure 4f–h) are much rougher and the fracture lines are shorter and multi-branched. From this, it is evidenced that the interactions between the MGO flakes and the polymer matrix were strong. This can also be considered as a confirmation that the MGO flakes were much more evenly distributed inside the epoxy matrix by noncovalent functionalization of POEGMA950-*b*-PAA. Besides, the interface between the epoxy matrix and the individual MGO layers was not clear (Figure 4f–h). This indicates that through the formation of a GO-dispersant-epoxy ternary molecular structure, the MGO layers were well dispersed in the epoxy matrix in the presence of POEGMA950-*b*-PAA (Figure 5).

TGA was utilized to investigate the thermal degradation process of products. The TGA curves of GO and MGO are shown in Figure 6a. For GO, there were three weight loss steps in the range of 25–600 °C. The absorbed water in GO's  $\pi$ -stacked structure contributed to the first step (below 100 °C); release of CO and CO<sub>2</sub> from the most labile oxygen-containing groups accounted for the second step (150–220 °C); and degradation of more stable oxygen-containing groups resulted in the third one (200–350 °C) [46]. The thermal degradation process of MGO is exactly the same as GO's (Figure 6a,b). Figure 6c shows the TGA curves of WEGC with different MGO content (0, 0.1, 0.5, and 1.0 wt.%). The residual char content ( $w_c$ ) was used to demonstrate the undecomposed materials

percentage at 600 °C (Figure 6c).  $T_{5\%}$  was defined as the initial degradation temperature.  $T_{max}$  was defined as the fastest mass loss temperature, and it was the peak temperature in the derivative curve of TGA (Figure 6d). As presented in Figure 6c, the degradation temperature and the residual char content is increased with an increase in the MGO content (the  $T_{5\%}$  and  $T_{max}$  increased 4–11 °C, and the  $w_c$  increased from 6.13% to 10.64% with an increase in MGO content of 0 wt.% to 1.0 wt.%). Other researchers have reported similar improvements in thermal properties with the presence of MGO [47]. It was suggested that the observed increase in thermal resistance resulted from the fact that nano-sized MGO layers, 1–2 nm thick, could sustain high temperature, retard heat diffusion into the epoxy matrix, and confine the motions of polymer chains.

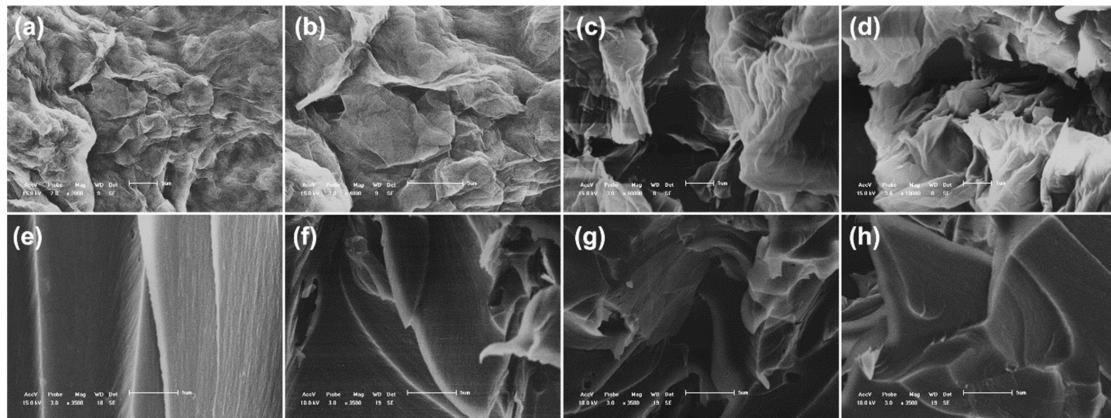


**Figure 4.** Typical scanning electron microscopy (SEM) images of (a,b) GO and (c,d) MGO; and the fracture surface SEM images of (e) WEGC-G0 (WEGC with no addition of GO), (f) WEGC-G1 (WEGC with 0.1 wt.% GO), (g) WEGC-G5 (WEGC with 0.5 wt.% GO), and (h) WEGC-G10 (WEGC with 1.0 wt.% GO).

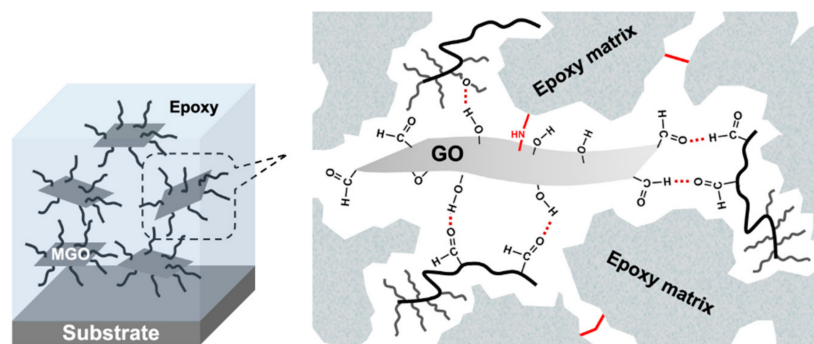


**Figure 5.** Schematic illustration of the dispersed mechanism of GO.

The anticorrosion properties of the pure epoxy coating (WEGC-G0) and epoxy-GO coatings (WEGC-G1, WEGC-G5, and WEGC-G10) were investigated by salt spray tests. As presented in Figure 7a, there was significant rust, blisters, and corrosion products on WEGC-G0 after 300 h of exposure to the accelerated conditions of the salt spray chamber. Furthermore, the corrosion products extended around the scratch, demonstrating the poor anticorrosion properties of WEGC-G0 (pure epoxy coatings). The WEGC with different contents of MGO showed different behaviors. For WEGC-G1, there was a small number of blisters and rust spots (small in size) (Figure 7b). For WEGC-G5, there were only very few rust spots, and no blisters were found after the 300 h test (Figure 7c). For WEGC-G10, the extent of corrosion was moderate, with the corrosion products predominantly appearing near the scribe of the coating (Figure 7d). This poor performance of WEGC-G10 may result from poor dispersion of MGO in the epoxy matrix when the MGO content is set too high, resulting in more pores or coating defects.

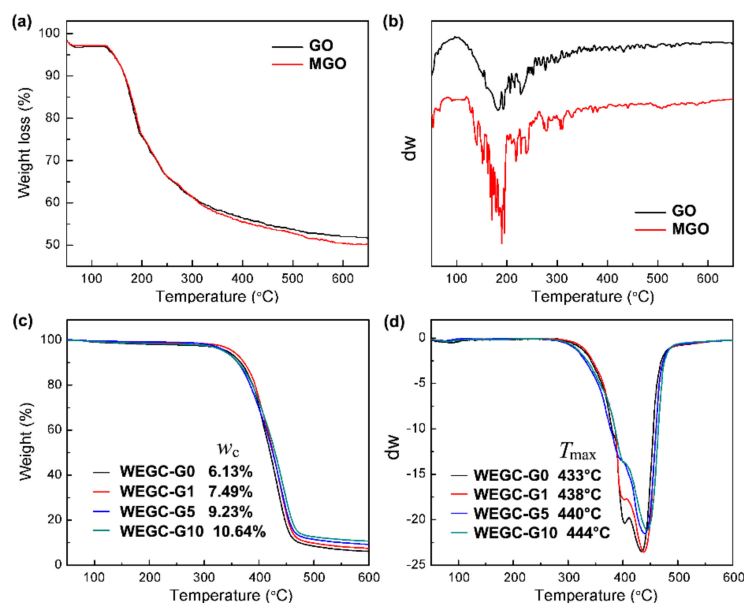


**Figure 6.** The thermogravimetric analysis (TGA) curves of (a) GO, MGO, and (c) WEGC; the derivative curve of TGA of (b) GO, MGO, and (d) WEGC.

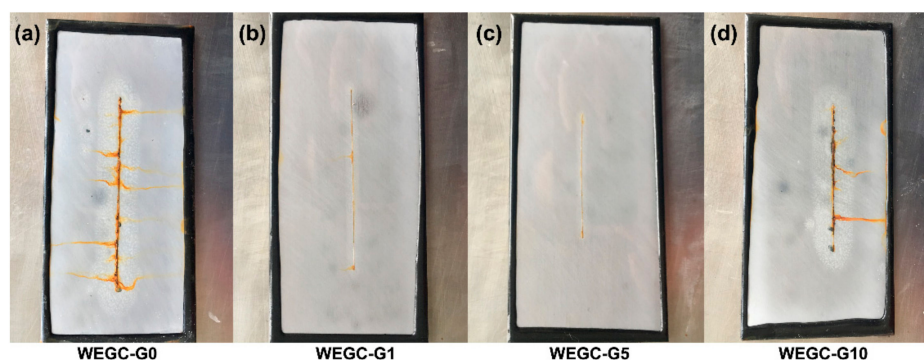


**Figure 7.** The images of samples after 300 h of exposure to the accelerated conditions of a salt spray chamber.

The barrier properties of the coatings were also investigated by determining the water absorption rates. As presented in Figure 8, the pure epoxy coating (WEGC-G0) had the highest water absorption rate after the 24 h test (4.65%), demonstrating the poor barrier properties of WEGC-G0. Initially, the water absorption rate gradually reduced with the addition of MGO (WEGC-G1: 4.24%, WEGC-G5: 3.62%). These findings indicate that the addition of well-dispersed MGO nanosheets can prevent water from permeating into the WEGC. However, the water absorption rate of WEGC-G10 was 4.42%, greater than that of WEGC-G5, which may have resulted from agglomeration of MGO. A schematic illustration of the GO-assisted anticorrosion mechanism is shown in Figure 9. With the presence of well-dispersed MGO nanosheets, the diffusion pathway of a corrosive substance (e.g., oxygen, water and corrosive ions) in an epoxy matrix will be significantly lengthened. As such, the barrier property of the coating will be greatly enhanced. In the case of WEGC-G5, the stable dispersion of MGO in the epoxy matrix created a cross-sectional structure that was denser than both the other WEGC coatings and the pure epoxy coating. Thus, WEGC-G5 exhibited excellent corrosion protection performance. This outcome is consistent with the conclusions drawn from SEM, XRD, and the salt spray test.

The adhesion of WEGC to Q235 steel was determined using a pull-off adhesion tester. As shown in Figure 10 and Table 1, the presence of MGO effectively improved the adhesion of the coatings. Initially, the adhesion of the coatings increased with the increments in MGO content. The highest

adhesion strength improvement (7.92 MPa) was obtained when 0.5 wt.% of MGO was added. In this case, POEGMA950-*b*-PAA acted as both the dispersant of GO and as a bridge for loading the GO and epoxy matrix. Thus, the addition of MGO can significantly enhance the adhesion properties of WEGC coatings. However, when the MGO content reached 1.0 wt.%, the adhesion strength decreased, with WEGC-G10 exhibiting an adhesion strength value of 4.50MPa. This indicated that there was some layer structure of the agglomerated MGO in the WEGC with higher MGO content. It is well known that not only does the block ability have an important role in the anticorrosion ability of coatings, but also the adhesion [48]. Consequently, using MGO to enhance the adhesion of coatings to protected metals is a useful approach for improving the anticorrosion performance of coatings.

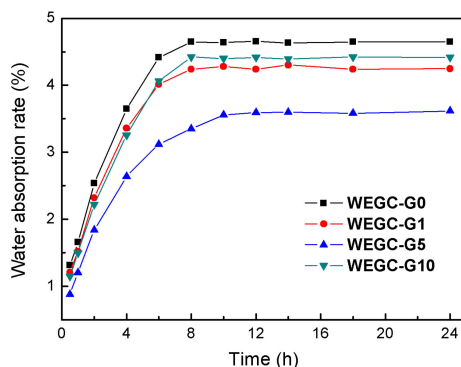


Figure 8. Water absorption rate of the WEGC with different MGO content (0, 0.1, 0.5, and 1.0 wt.%).

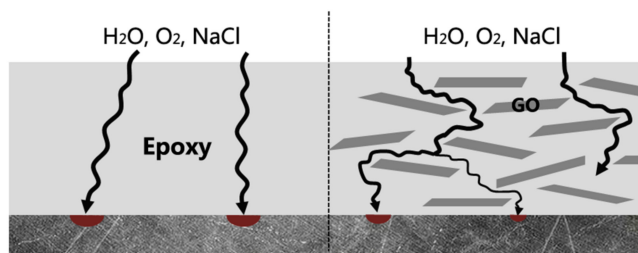


Figure 9. Schematic representation of corrosion protection mechanism of GO-epoxy coatings.

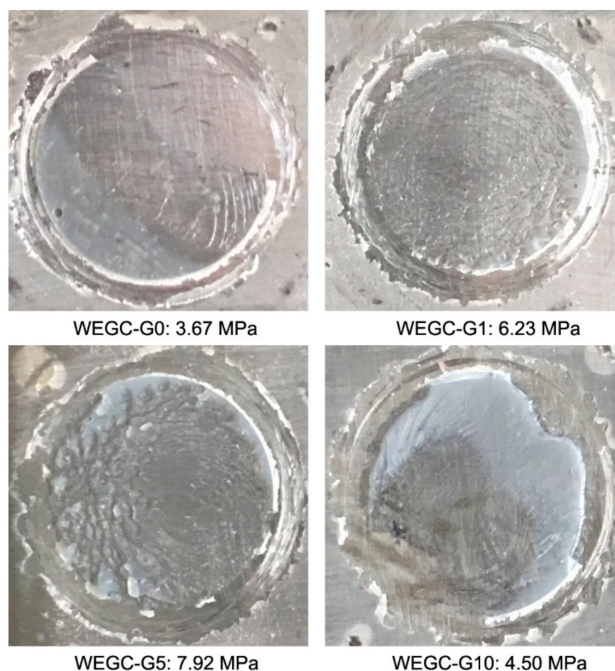


Figure 10. Pull-off test results for the WEGC applied on a steel surface.

**Table 1.** Pull-off test results of WEGC on Q235 steel.

Sample	WEGC-G0 (MPa)	WEGC-G1 (MPa)	WEGC-G5 (MPa)	WEGC-G10 (MPa)
1	3.54	6.21	8.15	4.31
2	3.82	6.45	7.88	4.58
3	3.65	6.02	7.74	4.61

#### 4. Conclusions

In this research, waterborne epoxy-GO coatings (WEGC) that used a block polymer as a dispersant of GO—wherein the block polymer was synthesized via RAFT polymerization of poly[oligo(ethylene glycol) methyl ether methyl acrylate] (POEGMA) and PAA—were successfully prepared. POEGMA950-*b*-PAA acted as an intercalation agent for both GO and the epoxy matrix. The XRD patterns and SEM photographs showed that: (1) MGO layers could be well-dispersed in the epoxy matrix and (2) the epoxy matrix could effectively contact MGO through the formation of a GO-dispersant-epoxy ternary molecular structure with the presence of POEGMA950-*b*-PAA. With the presence of well-dispersed MGO nanosheets, the diffusion pathway of corrosive substances (e.g., oxygen, water and corrosive ions) in an epoxy matrix will be significantly lengthened. As a consequence, the barrier property of such a coating will be greatly enhanced. TGA, salt spray tests, water absorption rate determination and pull-off tests showed that 0.5 wt.% MGO content brought the greatest enhancement in corrosion protection and barrier properties.

**Author Contributions:** Conceptualization, B.L.; Methodology, B.L.; Validation, B.L. and M.W.; Investigation, B.L., M.W., Y.L. (Ying Liang), Z.Z., G.R., and Y.L. (Yajun Liu); Formal Analysis, B.L.; Data Curation, B.L.; Visualization, B.L.; Supervision, S.W.; Project Administration, S.W.; Funding Acquisition, S.W.; Resources, S.W., and J.S.; Writing—Original Draft Preparation, B.L.; Writing—Review and Editing, B.L. and S.W.

**Funding:** This work is supported by the National Natural Science Foundation of China (Nos. 51408271, 51272100 and 51273073).

**Conflicts of Interest:** The authors declare no conflict of interest.

#### References

- Upadhyay, V.; Battocchi, D. Localized electrochemical characterization of organic coatings: A brief review. *Prog. Org. Coat.* **2016**, *99*, 365–377. [[CrossRef](#)]
- Zhang, J.T.; Hu, J.M.; Zhang, J.Q. Review on modern study methods of organic coatings. *Mater. Sci. Eng.* **2003**, *21*, 763–768.
- Cui, M.; Ren, S.; Chen, J.; Liu, S.; Zhang, G.; Zhao, H.; Wang, L.; Xue, Q. Anticorrosive performance of waterborne epoxy coatings containing water-dispersible hexagonal boron nitride (h-BN) nanosheets. *Appl. Surf. Sci.* **2017**, *397*, 77–86. [[CrossRef](#)]
- Wang, N.; Zhang, Y.N.; Chen, J.S.; Zhang, J.; Fang, Q.H. Dopamine modified metal-organic frameworks on anti-corrosion properties of waterborne epoxy coatings. *Prog. Org. Coat.* **2017**, *109*, 126–134. [[CrossRef](#)]
- Cao, L.; Jones, A.K.; Sikka, V.K.; Wu, J.; Di, G. Anti-icing superhydrophobic coatings. *Langmuir* **2009**, *25*, 12444–12448. [[CrossRef](#)]
- Wang, S.T.; Liu, K.S.; Yao, X.; Jiang, L. Bioinspired surfaces with superwettability: New insight on theory, design, and applications. *Chem. Rev.* **2005**, *115*, 8230–8293. [[CrossRef](#)]
- Guillaumin, V.; Landolt, D. Effect of dispersion agent on the degradation of a water borne paint on steel studied by scanning acoustic microscopy and impedance. *Corros. Sci.* **2002**, *44*, 179–189. [[CrossRef](#)]
- Wang, Y.G.; Chen, H.H.; Pei, S.F.; Zhang, T. Development of waterborne inorganic zinc silicate anticorrosion coatings. *Corros. Sci. Prot. Technol.* **2006**, *18*, 41–45. (In Chinese)
- Liu, M.; Mao, X.; Zhu, H.; Lin, A.; Wang, D. Water and corrosion resistance of epoxy-acrylic-amine waterborne coatings: Effects of resin molecular weight, polar group and hydrophobic segment. *Corros. Sci.* **2013**, *75*, 106–113. [[CrossRef](#)]
- Liu, T.; Li, J.; Li, X.; Qiu, S.; Ye, Y.; Yang, F.; Zhao, H. Effect of self-assembled tetraaniline nanofiber on the anticorrosion performance of waterborne epoxy coating. *Prog. Org. Coat.* **2019**, *128*, 137–147. [[CrossRef](#)]

11. He, Y.; Chen, C.; Xiao, G.; Zhong, F.; Wu, Y.; He, Z. Improved corrosion protection of waterborne epoxy/graphene coating by combining non-covalent and covalent bonds. *React. Funct. Polym.* **2019**, *137*, 104–115. [[CrossRef](#)]
12. Nie, J.; Liu, D.; Li, S.; Qiu, Z.; Ma, N.; Sui, G. Improved dispersion of the graphene and corrosion resistance of waterborne epoxy—Graphene composites by minor cellulose nanowhiskers. *J. Appl. Polym. Sci.* **2019**, *136*, 47631. [[CrossRef](#)]
13. Chen, C.; He, Y.; Xiao, G.; Zhong, F.; Li, H.; Wu, Y.; Chen, J. Synergistic effect of grapheme oxide@phosphate-intercalated hydrotalcite for improved anti-corrosion and self-healable protection of waterborne epoxy coating in salt environments. *J. Mater. Chem. C* **2019**, *7*, 2318–2326. [[CrossRef](#)]
14. Ding, J.H.; Rahman, O.; Peng, W.J.; Dou, H.M.; Yu, H.B. A novel hydroxyl epoxy phosphate monomer enhancing the anticorrosive performance of waterborne graphene/epoxy coatings. *Appl. Surf. Sci.* **2018**, *427*, 981–991. [[CrossRef](#)]
15. Genzer, J.; Efimenko, K. Recent developments in superhydrophobic surfaces and their relevance to marine fouling: A review. *Biofouling* **2006**, *22*, 339–360. [[CrossRef](#)]
16. Zhang, Z.X.; Zhang, T.; Zhang, X.; Xin, Z.X.; Deng, X.; Prakashan, K. Mechanically stable superhydrophobic polymer films by a simple hot press lamination and peeling process. *RSC Adv.* **2016**, *6*, 12530–12536. [[CrossRef](#)]
17. Novoselov, K.S.; Geim, A.K.; Morozov, S.V.; Jiang, D.; Zhang, Y.; Dubonos, S.V.; Grigorieva, I.V.; Firsov, A.A. Electric field effect in atomically thin carbon films. *Science* **2004**, *306*, 666–669. [[CrossRef](#)] [[PubMed](#)]
18. Ramezanzadeh, B.; Moghadam, M.M.; Shohani, N.; Mahdavian, M. Effects of highly crystalline and conductive polyaniline/graphene oxide composites on the corrosion protection performance of a zinc-rich epoxy coating. *Chem. Eng. J.* **2017**, *320*, 363–375. [[CrossRef](#)]
19. Chang, C.H.; Huang, T.C.; Peng, C.W.; Yeh, T.C.; Lu, H.I.; Hung, W.I.; Weng, C.J.; Yang, T.I.; Yeh, J.M. Novel anticorrosion coatings prepared from polyaniline/graphene composites. *Carbon* **2012**, *50*, 5044–5051. [[CrossRef](#)]
20. Posner, R.; Ozcan, O.; Grundmeier, G. Water and ions at polymer/metal interfaces. In *Design of Adhesive Joints under Humid Conditions*; da Silva, L.F.M., Sato, C., Eds.; Springer: Berlin, Germany, 2013; pp. 21–52.
21. Monetta, T.; Acquesta, A.; Bellucci, F. Graphene/epoxy coating as multifunctional material for aircraft structures. *Aerospace* **2015**, *2*, 423–434. [[CrossRef](#)]
22. Ganguli, S.; Roy, A.K.; Anderson, D.P. Improved thermal conductivity for chemically functionalized exfoliated graphite/epoxy composites. *Carbon* **2008**, *46*, 806–817. [[CrossRef](#)]
23. Gu, L.; Liu, S.; Zhao, H.; Yu, H. Facile preparation of water-dispersible graphene sheets stabilized by carboxylatedoligoanilines and their anticorrosion coatings. *ACS Appl. Mater. Interfaces* **2015**, *7*, 17641–17648. [[CrossRef](#)] [[PubMed](#)]
24. Zhu, K.; Li, X.; Wang, H.; Li, J.; Fei, G. Electrochemical and anti-corrosion behaviors of water dispersible graphene/acrylic modified alkyd resin latex composites coated carbon steel. *J. Appl. Polym. Sci.* **2017**, *134*, 44445. [[CrossRef](#)]
25. Jackson, M.; Kaushik, M.; Nazarenko, S.; Ward, S.; Maskell, R.; Wiggins, J. Effect of free volume hole-size on fluid ingress of glassy epoxy networks. *Polymer* **2011**, *52*, 4528–4535. [[CrossRef](#)]
26. Ding, R.; Li, W.H.; Wang, X.; Gui, T.J.; Li, B.J.; Han, P.; Tian, H.W.; Liu, A.; Wang, X.; Liu, X.J.; et al. In-situ reduction and deposition of Ag nanoparticles on black phosphorus nanosheets co-loaded with graphene oxide as a broad spectrum photocatalyst for enhanced photocatalytic performance. *J. Alloy. Compd.* **2018**, *764*, 1039–1055. [[CrossRef](#)]
27. Verdejo, R.; Bernal, M.M.; Romasanta, L.J.; Lopez-Manchado, M.A. Graphene filled polymer nanocomposites. *J. Mater. Chem.* **2011**, *21*, 3301–3310. [[CrossRef](#)]
28. Qiu, S.H.; Liu, G.; Li, W.; Zhao, H.C.; Wang, L.P. Noncovalent exfoliation of graphene and its multifunctional composite coating with enhanced anticorrosion and tribological performance. *J. Alloy. Compd.* **2018**, *747*, 60–70. [[CrossRef](#)]
29. Morsch, S.; Lyon, S.; Greensmith, P.; Smith, S.D.; Gibbon, S.R. Water transport in an epoxy-phenolic coating. *Prog. Org. Coat.* **2015**, *78*, 293–299. [[CrossRef](#)]
30. Sharma, J.; Tewari, K.; Arya, R.K. Diffusion in polymeric systems—A review on free volume theory. *Prog. Org. Coat.* **2017**, *111*, 83–92. [[CrossRef](#)]

31. Hayatgheib, Y.; Ramezanzadeh, B.; Kardar, P.; Mahdavian, M. A comparative study on fabrication of a highly effective corrosion protective system based on graphene oxide-polyanilin nanofibers/epoxy composite. *Corros. Sci.* **2018**, *133*, 358–373. [[CrossRef](#)]
32. Ramezanzadeh, B.; Niroumandrad, S.; Ahmadi, A.; Mahdavian, M.; Moghadam, M.H.M. Enhancement of barrier and corrosion protection performance of an epoxy coating through wet transfer of amino functionalized graphene oxide. *Corros. Sci.* **2016**, *103*, 283–304. [[CrossRef](#)]
33. Yu, C.; Chen, Q.; Wang, A.; Zhou, X.; Wu, S.; Ran, Q. Improved dispersibility of multi-wall carbon nanotubes with reversible addition-fragmentation chain transfer polymer modification. *Polym. Int.* **2015**, *64*, 1219–1224. [[CrossRef](#)]
34. Qiao, M.; Wu, S.S.; Wang, Y.W.; Ran, Q.P. Brush-like block copolymer synthesized via RAFT polymerization for graphene oxide aqueous suspensions. *RSC Adv.* **2017**, *7*, 4776–4782. [[CrossRef](#)]
35. Marcano, D.C.; Kosynkin, D.V.; Berlin, J.M.; Sinitskii, A.; Sun, Z.; Slesarev, A.; Alemany, L.B.; Lu, W.; Tour, J.M. Improved synthesis of graphene oxide. *ACS Nano.* **2010**, *4*, 4806–4814. [[CrossRef](#)]
36. *ASTM B117-18 Standard Practice for Operating Salt Spray (Fog) Apparatus*; ASTM International: West Conshohocken, PA, USA, 2018; Volume 03.02.
37. *ASTM D714-02 Standard Test Method for Evaluating Degree of Blistering of Paints*; ASTM International: West Conshohocken, PA, USA, 2017; Volume 06.01.
38. *ASTM D4541-17 Standard Test Method for Pull-Off Strength of Coatings Using Portable Adhesion Testers*; ASTM International: West Conshohocken, PA, USA, 2017; Volume 06.02.
39. Namvari, M.; Namazi, H. Sweet graphene I: Toward hydrophilic graphen nanosheets via click grafting alkyne-saccharides onto azide-functionalized graphene oxide. *Carbohydr. Res.* **2014**, *396*, 1–8. [[CrossRef](#)]
40. Thomsen, C.; Reich, S. Doable resonant Raman scattering in graphite. *Phys. Rev. Lett.* **2000**, *85*, 5214–5217. [[CrossRef](#)] [[PubMed](#)]
41. Kundu, A.; Nandi, S.; Das, P.; Nandi, A.K. Fluorescent graphene oxide via polymer grafting: An efficient nanocarrier for both hydrophilic and hydrophobic drugs. *ACS Appl. Mater. Interfaces* **2015**, *7*, 3512–3523. [[CrossRef](#)]
42. Zhang, Q.; Li, Q.L.; Xiang, S.; Wang, Y.; Wang, C.; Jiang, W.; Zhou, H.; Yang, Y.W.; Tang, J. Covalent modification of graphene oxide with polynorbornene by surface-initiated ring-opening metathesis polymerization. *Polymer* **2014**, *55*, 6044–6050. [[CrossRef](#)]
43. Jiang, T.; Kuila, T.; Kim, N.H.; Lee, J.H. Effects of surface-modified silica nanoparticles attached graphene oxide using isocyanate-terminated flexible polymer chains on the mechanical properties of epoxy composites. *J. Mater. Chem. A* **2014**, *2*, 10557–10567. [[CrossRef](#)]
44. Alexandre, M.; Dubois, P. Polymer-layered silicate nanocomposites: preparation, properties and uses of a new class of materials. *Mater. Sci. Eng. R* **2000**, *28*, 1–63. [[CrossRef](#)]
45. Roghani-Mamaqani, H.; Haddadi-Asl, V.; Khezri, K.; Salami-Kalajahi, M.; Najafi, M. Kinetic study of styrene atom transfer radical polymerization from hydroxyl groups of graphen nanoplalelets: Heterogeneities in chains and graft densities. *Polym. Eng. Sci.* **2015**, *55*, 1720–1732. [[CrossRef](#)]
46. Wang, Z.; Wei, P.; Qian, Y.; Liu, J. The synthesis of a novel graphene-based inorganic-organic hybrid flame retardant and its application in epoxy resin. *Compos. Part B* **2014**, *60*, 341–349. [[CrossRef](#)]
47. Neetika, G.; Kumar, D.; Tomar, S.K. Thermal behaviour of chemically synthesized polyanilines/polystyrene sulphonic acid composites. *Int. J. Mater. Chem.* **2012**, *2*, 79–85. [[CrossRef](#)]
48. Shreepathi, S.; Naik, S.M.; Vattipalli, M.R. Water transportation through organic coatings: Correlation between electrochemical impedance measurements, gravimetry, and water vapor permeability. *J. Coat. Technol. Res.* **2011**, *9*, 411–422. [[CrossRef](#)]

